Available online at www.sciencedirect.com
ScienceDirect
Journal of Theoretical Biology 242 (2006) 265–279
Journal of Theoretical Biology
www.elsevier.com/locate/yjtbi

Actin filament branching and protrusion velocity in a simple 1D model of a motile cell

Adriana T. Dawes[a,c,*], G. Bard Ermentrout[b], Eric N. Cytrynbaum[a,c], Leah Edelstein-Keshet[a,c]

[a]*Department of Mathematics, University of British Columbia, Vancouver, BC, Canada V6T 1Z2*
[b]*Department of Mathematics, University of Pittsburgh, Pittsburgh, PA 15260, USA*
[c]*Institute of Applied Mathematics, University of British Columbia, Vancouver, BC, Canada V6T 1Z2*

Received 19 October 2005; received in revised form 17 February 2006; accepted 22 February 2006
Available online 4 April 2006

Abstract

We formulate and analyse a 1D model for the spatial distribution of actin density at the leading edge of a motile cell. The model incorporates nucleation, capping, growth and decay of actin filaments, as well as retrograde flow of the actin meshwork and known parameter values based on the literature. Using a simplified geometry, and reasonable assumptions about the biochemical processes, we derive PDEs for the density of actin filaments and their tips. Analytic travelling wave solutions are used to predict how the speed of the cell depends on rates of nucleation, capping, polymerization and membrane resistance. Analysis and simulations agree with experimental profiles for measured actin distributions. Extended versions of the model are studied numerically. We find that our model produces stable travelling wave solutions with reasonable cell speeds. Increasing the rate of nucleation of filaments (by the actin related protein Arp2/3) or the rate of actin polymerization leads to faster cell speed, whereas increasing the rate of capping or the membrane resistance reduces cell speed. We consider several variants of nucleation (spontaneous, tip, and side branching) and find best agreement with experimentally measured spatial profiles of filament and tip density in the side branching case.

Keywords: Cell motility; Mathematical model; Actin dynamics; Lamellipod

1. Introduction

1.1. Cell motility

Animal cells move in response to an external signal by remodelling their cytoskeleton, composed of the abundant biopolymer, actin (Kurner et al., 2004). The motility of these cells is essential in embryogenesis, development, immune surveillance, wound healing, and many other cell functions (Tojima and Ito, 2004; Mandato and Bement, 2003). It is also implicated in disease processes such as rheumatoid arthritis and metastatic cancer (Lambrechts et al., 2004).

It is currently accepted that protrusion of the cell at its leading edge is mediated by actin filament tips pushing on the membrane. This results in extension of a long, flat, actin-rich protrusion called a lamellipod (Pollard and Borisy, 2003; Small et al., 2002). Actin filaments are polarized, and grow fastest by adding monomers at their plus (also called "barbed") ends, directed mainly toward the cell membrane. One mechanism that has been proposed to explain the force generated by polymerization of monomers at these ends is the thermal ratchet model (Mogilner and Oster, 1996, 2003). In order to limit potentially explosive elongation of filaments, capping proteins bind to barbed ends and prevent growth (Schafer et al., 1996; Pantaloni et al., 2000). Polymerization ceases when barbed ends are capped. Actin filaments are broken down by depolymerization and other recycling mechanisms, so that the monomers can be recharged, and reused in promoting new growth at the leading edge of the cell. As filaments age, they become more prone to degradation. Hence, depolymerization dominates in the rear parts of the lamellipod structure.

*Corresponding author. Tel.: +1 604 822 2666; fax: +1 604 822 6074.
E-mail address: atdawes@math.ubc.ca (A.T. Dawes).

0022-5193/$ - see front matter © 2006 Elsevier Ltd. All rights reserved.
doi:10.1016/j.jtbi.2006.02.017

A small but distinct rearward flow of the actin meshwork has recently been observed in the lamellipodia of moving fish epidermal cells called *keratocytes* (Ponti et al., 2004; Jurado et al., 2005; Vallotton et al., 2005). Previously this had only been observed in slower moving cells such as fibroblasts (Ponti et al., 2005; Henson et al., 1999). In keratocytes, the lamellipod is separated from the cell body by a band rich in myosin II, a motor protein that binds to actin filaments and moves towards the barbed end of a filament (Svitkina and Borisy, 1999). Since most actin filaments in the lamellipod are oriented with their barbed ends in the direction of motion (Svitkina and Borisy, 1999), the interaction of myosin II with the actin filaments in the lamellipod causes a bulk flow of the actin meshwork away from the leading edge. Retrograde flow in keratocytes is smallest in the middle of the lamellipod (approximately $0.01\,\mu m\,s^{-1}$) increasing to approximately $0.05\,\mu m\,s^{-1}$ at the edges, in cells moving $0.2–0.3\,\mu m\,s^{-1}$.

Of great interest in the last decade is the complex Arp2/3, essential for cell motility and now known to nucleate new filaments. Arp2/3 undergoes activation at the leading edge, and then gives rise to new barbed ends that can grow into filaments. In previous years, there had been some debate whether Arp2/3 attaches to actin filament sides or to their barbed ends in order to nucleate new branches (Falet et al., 2002; Pantaloni et al., 2000). Some groups (Amann and Pollard, 2001; Fujiwara et al., 2002) favored Arp2/3 binding to sides, close to the tips of existing filaments. Existing technology does not allow direct imaging of Arp2/3 nucleation as it occurs in a motile cell, but a variety of other experimental observations and theoretical analyses (Carlsson et al., 2004) currently lead to strong support for side branching off pre-existing filaments.

Estimates for biochemical parameters such as capping and nucleation rates have been based on results of in vitro experiments using cell extracts (at protein concentrations similar to those found in cytoplasm), but not intact cells (Pollard et al., 2000). Thus, estimated biochemical rates and parameter values are still subject to experimental refinement. At the same time, visualization of the actin network (Bailly et al., 1999; Svitkina and Borisy, 1999) has allowed measurement of densities of polymerized actin, of filaments, and even of their barbed ends as a function of distance away from the leading edge. As yet, no theoretical treatment of these measured densities and the filament dynamics that account for these densities has been completed. This forms the subject of our paper.

In this paper, our aim is to derive and investigate a simple description of actin filament nucleation, capping, growth and depolymerization in a 1D model of the lamellipod. We ask whether the known events described above can account for (a) membrane speed, (b) the density profiles of filaments and ends, and (c) dependence of speed on biochemical parameters. We base the model on known biochemical parameters and use it to infer those that are not easy to measure.

1.2. Previous modelling efforts

A number of models have been proposed to investigate actin dynamics in motile cells. Some models focus primarily on the actin monomer cycle and actin polymerization at the leading edge (Mogilner and Edelstein-Keshet, 2002; Grimm et al., 2003). Using a 1D model, Mogilner and Edelstein-Keshet (2002) show how membrane speed depends on barbed ends and ATP-actin monomer concentration at the leading edge of a cell. Grimm et al. (2003) make predictions regarding the shape of the leading edge. Both papers employ a force–velocity relationship as the basis for membrane protrusion, but neither is concerned with the profiles of actin density or the biochemistry of branching mediated by Arp2/3. Carlsson (2001) uses a stochastic 3D model to simulate the growth of an actin network against an obstacle. Other models have been proposed for actin length distribution in a 1D strip of the lamellipod. Edelstein-Keshet and Ermentrout (2000) focus on cutting and severing of filaments rather than branching. In a more recent paper Carlsson et al. (2004) combine in vitro experimental work with modelling of actin dynamics in a well-mixed, spatially homogeneous setting and find that side branching provides the best fit to experimental data.

Our model complements previous approaches in several respects. First, (like Edelstein-Keshet and Ermentrout, 2000 but unlike Mogilner and Edelstein-Keshet, 2002) we are concerned with spatial distribution of actin filaments and their barbed ends; our model can then be used to compare against actin density distributions observed in experiments. We explore actin density evolution in a simplified 1D geometry (see Fig. 1) to investigate the interplay between filament branching, growth, and decay in proximity to the leading edge. Second, as in many previous models, we use both analytic and simulation techniques. However, since we study a minimal model, it is possible to find (in the simplest case) explicit forms of travelling waves that represent the steady state motion of a motile cell. This leads to analytic expressions for experimentally measurable quantities such as protrusion velocity and spatial density profiles in terms of kinetic parameters such as rates of capping, nucleation, polymerization and disassembly of actin. A primary focus is on the role of Arp2/3 in initiating branches on filaments. By explicitly incorporating Arp2/3 activation at the leading edge, its diffusion, and its role as a nucleator of new actin filament tips that push the membrane, we can investigate consequences of distinct types of branching on the resultant actin dynamics, distribution and cell speed.

2. Biological background

Actin polymerizes from its monomeric form (G-actin) to a filamentous form (F-actin). Filamentous actin is polar, with faster growth due to monomer addition at the barbed end than the pointed end. Polymerization of ATP-actin

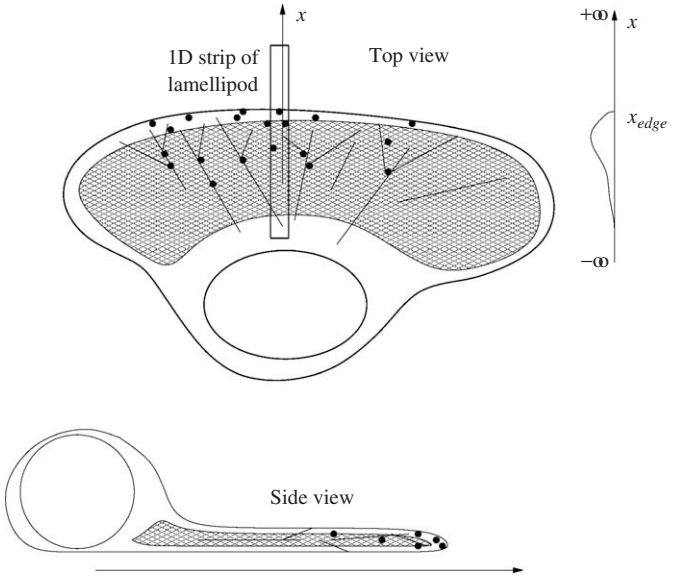

Fig. 1. Geometry of the model. Shown is a schematic diagram of a moving keratocyte. (The arrow indicates the direction of filament growth and the direction of protrusion. Retrograde flow is in the opposite direction.) The boundary $+\infty$ is ahead of the cell, $-\infty$ is at the rear of the lamellipod (a thin sheet-like structure that forms at the leading edge of the cell). A typical distribution of actin filament density predicted by our model (and seen experimentally) is shown along the axis to the right.

monomers at the barbed ends is rapid. The ATP nucleotide is later degraded to ADP, which acts as a marker for older parts of an actin filament. Polymerization of actin in the lamellipod is tightly regulated by many factors that cap, nucleate, and depolymerize the filaments (Wood and Martin, 2002; Small et al., 2002).

Regulation of the number of actively polymerizing barbed ends is necessary for efficient cell protrusion; otherwise the pool of available actin monomers would be quickly depleted by a large number of polymerizing barbed ends. Capping protein binds to the barbed ends of actin filaments with high affinity and prevents further polymerization activity (Feinberg et al., 1998). It is thought that tips are protected from capping protein in a zone near the leading edge (DiNubile and Huang, 1997; Huang et al., 1999).

Filaments are disassembled by simple loss of monomers, by cutting, or by some combination thereof. The protein ADF/cofilin accelerates filament breakup, so that freed monomers can be recycled to the leading edge to maintain cell motion. Experiments suggest that depolymerization tends to occur more frequently away from the leading edge (Vallotton et al., 2004), where filaments are more likely to be in the ADP-actin form.

It is known that Arp2/3, essential for cell motility (Bailly et al., 2001), is responsible for the branched actin network seen in the lamellipodium (Suetsugu et al., 2002). It is not clear if Arp2/3 must remain bound to the membrane, or if it diffuses away from the membrane before binding to a filament and nucleating a new barbed end. Once activated by membrane bound proteins such as WASp or ActA, Arp2/3 can associate with an existing filament to nucleate a new barbed end at 70° to the parent filament (Amann and Pollard, 2001). Arp2/3 is incorporated into the filament during the nucleation process.

2.1. Survey of experimental techniques

A number of recent papers present experimental data concerning the structure and composition of the actin meshwork in the lamellipod of different types of motile cells. The two techniques used for imaging are fluorescence and electron microscopy.

Using fluorescently labelled actin and Arp2/3 in live cells, it was found that polymerization of labelled actin monomers occurs almost exclusively at the leading edge of motile cells (Redmond and Zigmond, 1993; Svitkina et al., 1997; Ponti et al., 2004; Bailly et al., 1999), Moreover, Arp2/3 is also incorporated into the actin meshwork near the leading edge (Falet et al., 2002; Svitkina and Borisy, 1999; Bailly et al., 1999).

Electron micrographs of fixed cells that have gold particles attached to Arp2/3 and barbed ends provide an absolute measure of the number of free tips and branch points in some small region near the leading edge. These measures are consistent with fluorescence experiments, showing most barbed ends within 0.5 μm of the leading edge and Arp2/3 incorporated into the meshwork over 2–3 μm near the leading edge (Bailly et al., 1999; Svitkina and Borisy, 1999). Experiments using both live and fixed imaging of motile cells have determined that approximately 80% of filaments up to 8 μm away from the leading edge are oriented with their barbed ends pointing toward the leading edge (Svitkina et al., 1997; Small et al., 1995; Verkhovsky et al., 2003).

3. The mathematical model

In this section, we specify the assumptions made in the development of models to investigate cell motility. We then develop a model to determine how cell motility is affected by processes such as branching and capping. We ask the following questions:

(A) Can a minimal model for actin filament nucleation, capping, and depolymerization account for observed typical density profiles in a rapidly moving cell?
(B) Under what conditions can this actin profile sustain travelling wave solutions typical of steady state cell motion?
(C) Given the thermal ratchet mechanism for membrane motion driven by actin filaments, how does membrane speed depend on biochemical parameters such as nucleation, capping, and depolymerization rates?
(D) How would distinct nucleation mechanisms (spontaneous, tip branching, or filament side-branching) affect the observed density profiles and speeds?

Table 1
Definitions of model parameters and typical values based on biological literature

Parameter	Meaning	Value	Source
D_R	Diffusion rate of Arp2/3	$3\ \mu m^2\ s^{-1}$	Pollard et al. (2000)
v	Polymerization velocity	$0.3\ \mu m\ s^{-1}$	Pollard and Borisy (2003)
v_r	Retrograde flow rate	$0.01\ \mu m\ s^{-1}$	Vallotton et al. (2005))
η_0	Spontaneous nucleation rate	$100\ \mu m^{-1}\ s^{-1}$	Estimated in text
η_1	Nucleation rate: tip branching	$0.1\ s^{-1}$	Estimated in text
η_2	Nucleation rate: side branching	$1\ \mu m^{-1}\ s^{-1}$	Estimated in text
κ	Capping rate	$1\ s^{-1}$	Schafer et al. (1996)
δ	Depolymerization rate	$1/60–1/300\ s^{-1}$	Pollard and Borisy (2003)

(E) Can observed actin densities be used to infer or estimate any of the biochemical parameters?

Model variables are defined below. Table 1 lists parameters, their meanings and values assigned to them based on the literature or calculated in this paper.

3.1. Basic assumptions

The following simplifying assumptions are made in formulating the model.

1. The lamellipod is a thin flat sheet, approximately 10 μm long. Its vertical thickness (~200 nm, Abraham et al., 1999) is here ignored.
2. The domain is a one dimensional strip of lamellipod (see Fig. 1).
3. Forward protrusion of the leading edge occurs at a rate that depends on the number of barbed ends at the membrane. We mainly consider steady state motion for which the rate of membrane protrusion is constant.
4. The membrane provides constant resistance to movement.
5. Dynamic processes such as capping, branching and depolymerization are modelled using first order kinetics.
6. The actin dynamics of interest take place near the leading edge, assumed to be far from any physical barriers.
7. The number of barbed ends at the rear of the lamellipod is negligible.

Assumption 1 about the lamellipod geometry, made for analytical ease, is reasonable since the lamellipod is long and flat. Assumption 2 is a simplification. The 2D and 3D effects could be important, and will be examined in a later treatment. In Assumption 3 we use the thermal ratchet mechanism for membrane protrusion derived by Mogilner and Oster (1996). Here we simplify the dependence of the membrane speed on the number of barbed ends in Assumptions 3 and 4. Actin dynamics (Assumption 5) are likely to be more complicated than linear kinetics and we ignore saturation effects due to limited pools of the required proteins (i.e. Arp2/3 and capping proteins). Studies that measure actin incorporation using labelled monomers demonstrate that active actin polymerization takes place at the leading edge of motile cells. Since all uncapped barbed ends are capable of polymerization, Assumptions 6 and 7 are reasonable.

3.2. Definitions

We define the following variables and parameters:

$B(x,t)$	density of actively growing barbed ends, #/μm
$F(x,t)$	filament length density, $\mu m\ \mu m^{-1}$
$R(x,t)$	Arp2/3 concentration, scaled
x_{edge}	position of leading edge
c	membrane speed, $\mu m\ s^{-1}$
v	speed of tip growth, $\mu m\ s^{-1}$
v_r	speed of retrograde flow, $\mu m\ s^{-1}$
x	spatial coordinate
t	time coordinate
z	position relative to leading edge in moving coordinates

3.3. Description of the model

The model keeps track of freely polymerizing barbed ends (B), filament length density (F) and the density of Arp2/3 (R).

We make the following additional assumptions:

1. Nucleation events (spontaneous, tip or side branching) require active Arp2/3.
2. Arp2/3 is activated only at the membrane where it interacts with membrane-associated proteins of the SCAR/WASp family.
3. Arp2/3 is used up by nucleation events.
4. All filaments point toward the membrane and grow in the direction of motion at a constant rate of polymerization, v.
5. At the leading edge, we assume that there are no filaments and that Arp2/3 is generated by a constant source.
6. Barbed ends and filaments experience a constant retrograde flow away from the leading edge.

7. Arp2/3 diffuses in the cell and possibly advects due to the motion of the leading edge and/or retrograde flow. Here we assume a constant retrograde flow.

We assume that the rate of increase of barbed ends due to nucleation by Arp2/3 (in full generality) is $\eta_0 R + \eta_1 RB + \eta_2 RF$, where η_0, the spontaneous de novo nucleation rate, η_1 and η_2, the tip and side branching rates, are here approximated as constants (possibly zero). Barbed ends are capped by capping protein that stops polymerization from occurring at that tip. We take barbed end loss due to capping as $-\kappa B$ where κ is a per tip mean rate of capping. Filaments and barbed ends flow away from the leading edge at rate of retrograde flow v_r and barbed ends also move at the speed of polymerization v, which we assume to be constant. Arp2/3 is generated at the leading edge at a constant rate, diffuses freely on the domain with diffusion rate D_R and is used up by nucleation events. We consider three possible events: spontaneous nucleation, tip branching, and filament side branching (each proportional to Arp2/3 concentration, with rates $\eta_0, \eta_1, \eta_2 \geq 0$, respectively).

Forward protrusion of the membrane (and/or retrograde flow of the actin meshwork) leads to bulk cytoplasmic flow that carries with it soluble factors such as Arp2/3. Advection terms with speeds related to these flow velocities thus appear in the equation for Arp2/3. The level of Arp2/3, R, is scaled with respect to its maximal value at the cell membrane so R is dimensionless and ranges between 0 and 1. Filaments grow by elongation at a rate that depends on tip velocity: the rate of filament length density gain by polymerization is Bv. We here model filament loss as a simple linear decay, i.e. $-F\gamma$ where $1/\gamma$ is mean filament lifetime. Note that this is general degradation, not merely depolymerization at the pointed end of the filament.

The model equations are

$$\frac{\partial B}{\partial t} = (v_r - v)\frac{\partial B}{\partial x} + \eta_0 R + \eta_1 RB + \eta_2 RF - \kappa B, \tag{1}$$

$$\frac{\partial R}{\partial t} = D_R \frac{\partial^2 R}{\partial x^2} - \eta_0 R - \eta_1 RB - \eta_2 RF + v_{bulk}\frac{\partial R}{\partial x}, \tag{2}$$

$$\frac{\partial F}{\partial t} = v_r \frac{\partial F}{\partial x} + Bv - F\gamma, \tag{3}$$

where

$$v_{bulk} = \alpha_1 v_r - \alpha_2 x'_{edge}.$$

In these equations, first order spatial derivatives capture the retrograde flow and/or other convective processes such as tip motion. Only Arp2/3 diffuses and reacts (with actin) to form new barbed ends. We consider three limiting forms for the bulk advection, v_{bulk}, of Arp2/3 in which v_{bulk} is (i) precisely equal to forward membrane protrusion ($\alpha_1 = 0, \alpha_2 = 1$), (ii) determined only by retrograde flow ($\alpha_1 = 1, \alpha_2 = 0$) and (iii) a superposition of the two ($\alpha_1 = 1, \alpha_2 = 1$). Of these options, (iii) would be most realistic. For ease, we absorb the units and magnitude of the source of Arp2/3 at the membrane into the nucleation parameters η_i.

The corresponding boundary conditions are

$$B(-\infty, t) = 0, \tag{4}$$

$$R(-\infty, t) = 0, \tag{5}$$

$$R(x_{edge}, t) = R_0. \tag{6}$$

Since R is scaled with respect to its maximum value and the only source of active Arp2/3 is at the membrane, $R_0 = 1$.

We use a force–velocity relation based on the thermal ratchet mechanism (see Mogilner and Oster, 1996) to determine the speed of the membrane:

$$\frac{dx_{edge}}{dt} = (v - v_r)\exp\left(-\frac{\phi\delta}{k_B T B(x_{edge})}\right) = (v - v_r)\exp(-w/B(x_{edge})), \tag{7}$$

where ϕ is the force exerted by a single filament tip, δ is the filament length gained by the addition of a single monomer, k_B is the Boltzmann constant, T is temperature, and $w = \phi\delta/k_B T$ is assumed to be constant. We assume that barbed ends cannot cross the membrane. Eq. (7) means that, at the membrane, tips move more slowly than immediately further back, but capping prevents unlimited accumulation of tips at the membrane.

3.4. Analysis of travelling wave solutions: spontaneous branching

In this section, we consider the situation where barbed ends are formed only by spontaneous Arp2/3 nucleation events ($\eta_0 \neq 0$, $\eta_1 = \eta_2 = 0$). The model equations are

$$\frac{\partial B}{\partial t} = (v_r - v)\frac{\partial B}{\partial x} + \eta_0 R - \kappa B, \tag{8}$$

$$\frac{\partial R}{\partial t} = D_R \frac{\partial^2 R}{\partial x^2} - \eta_0 R + v_{bulk}\frac{\partial R}{\partial x}, \tag{9}$$

$$\frac{\partial F}{\partial t} = v_r \frac{\partial F}{\partial x} + vB - \gamma F, \tag{10}$$

with boundary conditions and edge motion as above.

We investigate whether this model can give rise to travelling wave solutions. We assume that the membrane moves to the right with constant speed c so that $x'_{edge} = c$. We designate our moving coordinate as $z = x - ct$, where $z = 0$ is the location of the cell membrane.

Transforming to moving coordinates $b(z) = B(x - ct, t)$, $r(z) = R(x - ct, t)$ and $f(z) = F(x - ct, t)$,

$$-c\frac{db}{dz} = (v_r - v)\frac{db}{dz} + \eta_0 r - \kappa b, \tag{11}$$

$$-c\frac{dr}{dz} = D_R \frac{d^2 r}{dz^2} - \eta_0 r + v_{bulk}\frac{dr}{dz}, \tag{12}$$

$$-c\frac{df}{dz} = v_r\frac{df}{dz} + vb - \gamma f, \tag{13}$$

with boundary conditions

$$b(-\infty) = 0, \tag{14}$$

$$r(-\infty) = 0, \tag{15}$$

$$f(0) = 0, \tag{16}$$

$$r(0) = R_0. \tag{17}$$

Eq. (12) is a second order linear ODE with constant coefficients and is thus fully solvable in explicit form. Consider solutions for r of the form $r = \bar{c}\exp(\lambda z)$. Substituting this expression into Eq. (12), we find the eigenvalues

$$\lambda_\pm = \begin{cases} \pm\sqrt{\dfrac{\eta_0}{D_R}} & \text{(i)}, \\ \dfrac{-(v_r+c) \pm \sqrt{(v_r+c)^2 + 4D_R\eta_0}}{2D_R} & \text{(ii)}, \\ \dfrac{-v_r \pm \sqrt{v_r^2 + 4D_R\eta_0}}{2D_R} & \text{(iii)}, \end{cases} \tag{18}$$

for the three cases, (i) $\alpha_1 = 0, \alpha_2 = 1$, (ii) $\alpha_1 = 1, \alpha_2 = 0$ and (iii) $\alpha_1 = 1, \alpha_2 = 1$. Here $\lambda_+ > 0$, $\lambda_- < 0$, and $\lambda_\pm$ are always real valued. Then,

$$r(z) = C_1 e^{\lambda_+ z} + C_2 e^{\lambda_- z}. \tag{19}$$

Since there is no active Arp2/3 far from the membrane ($r(-\infty) = 0$), $C_2 = 0$. We also specify $r(0) = R_0 = 1$ which makes $C_1 = R_0 = 1$. So our solution for r is

$$r(z) = R_0 e^{\lambda_+ z}. \tag{20}$$

Substituting the solution for r into Eq. (11) for barbed ends and using $b(-\infty) = 0$, we find the solution for b is

$$b(z) = \frac{\eta_0 R_0}{(v - v_r - c)\lambda_+ + \kappa} e^{\lambda_+ z}. \tag{21}$$

We now substitute the solution for b into Eq. (13). Since $f(0) = 0$, the solution for f is

$$f(z) = \frac{\eta_0 R_0 v}{((v - v_r - c)\lambda_+ + \kappa)((v_r + c)\lambda_+ - \gamma)}(e^{\gamma z/(v_r+c)} - e^{\lambda_+ z}). \tag{22}$$

The spatial profiles of B, R and F are shown in Fig. 2.

We can also determine an explicit expression for the membrane speed in the spontaneous branching case in terms of parameters. Using Eqs. (7) and (21), we obtain an implicit equation for the speed c,

$$\begin{aligned} c &= (v - v_r)\exp\left(-\frac{w}{b(0)}\right) \\ &= (v - v_r)\exp\left(-\frac{w(\lambda_+(v - v_r - c) + \kappa)}{\eta_0 R_0}\right). \end{aligned} \tag{23}$$

3.5. Tip and side branching

In the case of tip ($\eta_1 \neq 0$, $\eta_0 = \eta_2 = 0$) and side ($\eta_2 \neq 0$, $\eta_0 = \eta_1 = 0$) branching, Eqs. (1–3) is nonlinear and not easily solved using analytic techniques. To explore these two cases, we rely on numerical simulations.

4. Parameter values

A number of parameter values can be estimated directly from reported biological experiments. The following parameters are used as input to our model and produce the results shown in Figs. 2 and 3.

The polymerization velocity v of a barbed end is determined by measuring the net gain in length due to monomer addition over a measured period of time. Assuming actin monomers are freely available, a barbed end grows at approximately $v \approx 0.3\,\mu m\,s^{-1}$ (Pollard et al., 2000). The measured velocity of retrograde flow in the lamellipod of keratocytes ranges from 0.01 to $0.05\,\mu m\,s^{-1}$ (Jurado et al., 2005; Vallotton et al., 2005). Since our domain of interest is in the middle of the lamellipod, away from any edges, we use $v_r = 0.01\,\mu m\,s^{-1}$. When filaments are exposed to the concentration of ADF/cofilin found in cells, filaments disassemble at the rate of $\gamma \approx 1/30\,s^{-1}$ (Pollard and Borisy, 2003). At the concentration of capping protein usually found in cells, barbed ends are capped at a rate of $\kappa \approx 1\,s^{-1}$ (Schafer et al., 1996).

There are no direct observations of rates of Arp2/3 nucleation in motile cells. We wanted to compare the three types of branching mechanisms, in the hypothetical case that each acts on its own. Since each branching parameter (η_0, η_1, η_2) has a distinct set of units, to make this comparison, we picked values that would lead to a similar level of actin density at the leading edge.

For spontaneous branching alone ($\eta_1 = \eta_2 = 0$) at steady state locomotion, there should be a balance between nucleation and branching so that $\eta_0 R \approx \kappa B$. Since we have scaled the activated Arp2/3 concentration so that its maximal value is $R = 1$, the parameter η_0 is an effective maximal spontaneous nucleation rate. This rate is corrected by the fraction of Arp2/3 available in a given location, relative to that at the membrane. Experiments suggest there are approximately $B(0) = 100$ barbed ends along each micron of membrane at the leading edge (Bailly et al., 1999; Abraham et al., 1999). At steady state cell locomotion, using the known capping rate, this leads to the estimate $\eta_0 R_0 \approx \kappa B(0)$ so that $\eta_0 \approx 100\,\mu m^{-1}\,s^{-1}$. For side branching on its own ($\eta_0 = \eta_1 = 0$), the balance between branching and capping at the leading edge implies $\eta_2 RF \approx \kappa B$, leading to the estimate $\eta_2 = \kappa B(0)/FR$. We assume that at the leading edge, there is roughly one tip per $1\,\mu m$ length filament (an underestimate based on the ramified network), then $\eta_2 \approx 1\,\mu m^{-1}\,s^{-1}$. Finally, using the fact that average spacing between branch points is $0.1\,\mu m$ (Wiesner et al., 2003), we can determine an equivalent value of the branching

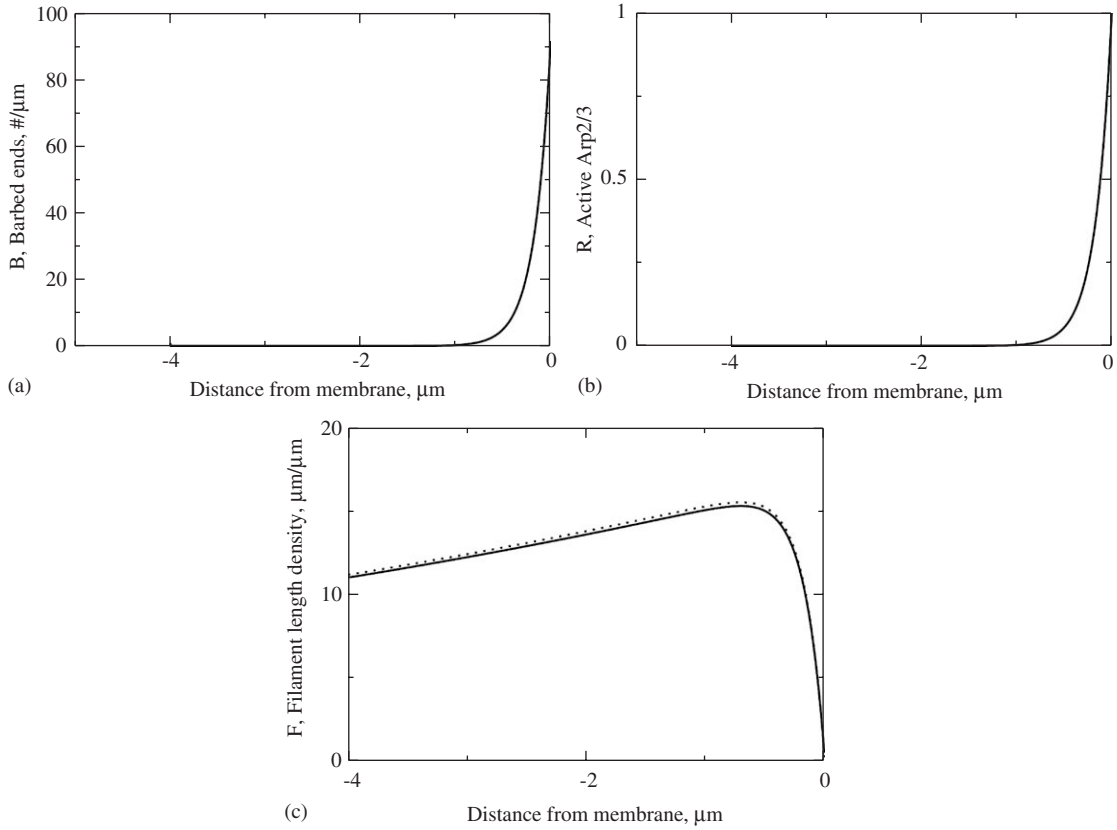

Fig. 2. Comparison of analytic and simulation results. Plot of analytic solution (solid line) of a travelling wave solution in the spontaneous branching case as determined in Section 3.4 using $\eta_0 = 100$, and other parameter values as given in Table 1. (a) Profile of barbed ends, (b) profile of Arp2/3 concentration, (c) filament length density profile over the region $-4 \le z \le 0$, where z is position in μm relative to the cell membrane. Spatial profiles in the absence of retrograde flow ($v_r = 0$) are so close as to be exactly superimposed in this figure. Also shown are the simulation results (dotted lines) discussed in Section 5. Analysis and simulations agree so closely that results superimpose in Fig. 2(a) and (b). Arbitrary initial density distributions converged, after some transient, to the steady state wave profile shown, indicating the stability of these travelling wave solutions. There is good agreement between the analytic result and the simulations, suggesting our numerical implementation is adequate for capturing the model dynamics.

parameter in the case of tip branching on its own, i.e. $\eta_1 \approx (1\,\mu\text{m}^{-1}\,\text{s}^{-1})(0.1\,\mu\text{m}) = 0.1\,\text{s}^{-1}$. This reasoning led us to adopt the set of approximately comparable branching rates:

$$\eta_0 \approx 100\,\mu\text{m}^{-1}\text{s}^{-1}, \quad \eta_1 \approx 0.1\,\text{s}^{-1}, \quad \eta_2 \approx 1\,\mu\text{m}^{-1}\,\text{s}^{-1}.$$

These values would produce a roughly similar leading edge density of actin if each of the three nucleation mechanisms were acting alone. Note that because in 1D the filament density is essentially dimensionless (length of filaments per unit distance), the units of η_0 and η_2 coincide.

The diffusion coefficient of an actin monomer, whose molecular weight is approximately 40 kDa, is $50\,\mu\text{m}^2\,\text{s}^{-1}$ in pure water but due to effects of electrolytes, other globular proteins, and possible non-specific binding to intracellular structures, it has been revised downwards to $5\,\mu\text{m}^2\,\text{s}^{-1}$ (James McGrath, Diffusion of actin monomers in the cell, ICAMS workshop on Biophysics of actin-based motility, Aspen Co, September 3–6, 2004, http://icam.ucop.edu/workshops.html). Since Arp2/3 has a molecular weight of approximately 220 kDa, we take its diffusion coefficient to be $D_R \approx 3\,\mu\text{m}^2\,\text{s}^{-1}$. These parameter values are compiled in Table 1.

5. Simulations

The model was simulated numerically using explicit (upwind differencing) for transport terms and centered differencing for diffusion terms. Where possible, the simulation results were tested against analytical predictions of Section 3.4. The discretized equations of the model in moving coordinates, coded in C, were iterated on a 1D domain 20 μm in length with step size $\Delta x = 0.005\,\mu\text{m}$ and an appropriate time step Δt for stability.

The simulations can be initiated from arbitrary initial distributions of the variables, but we started all runs with a non-zero density of barbed ends to assure propagation in all branching variants. Results are shown for a linear initial profile of barbed ends. (All other variables were set to 0 at $t = 0$. The diffusion of Arp2/3 from the edge then leads to nucleation of new tips, whose growth fills the domain with filaments.) We tested the simulations with a variety of other initial barbed end distribution profiles (with compact

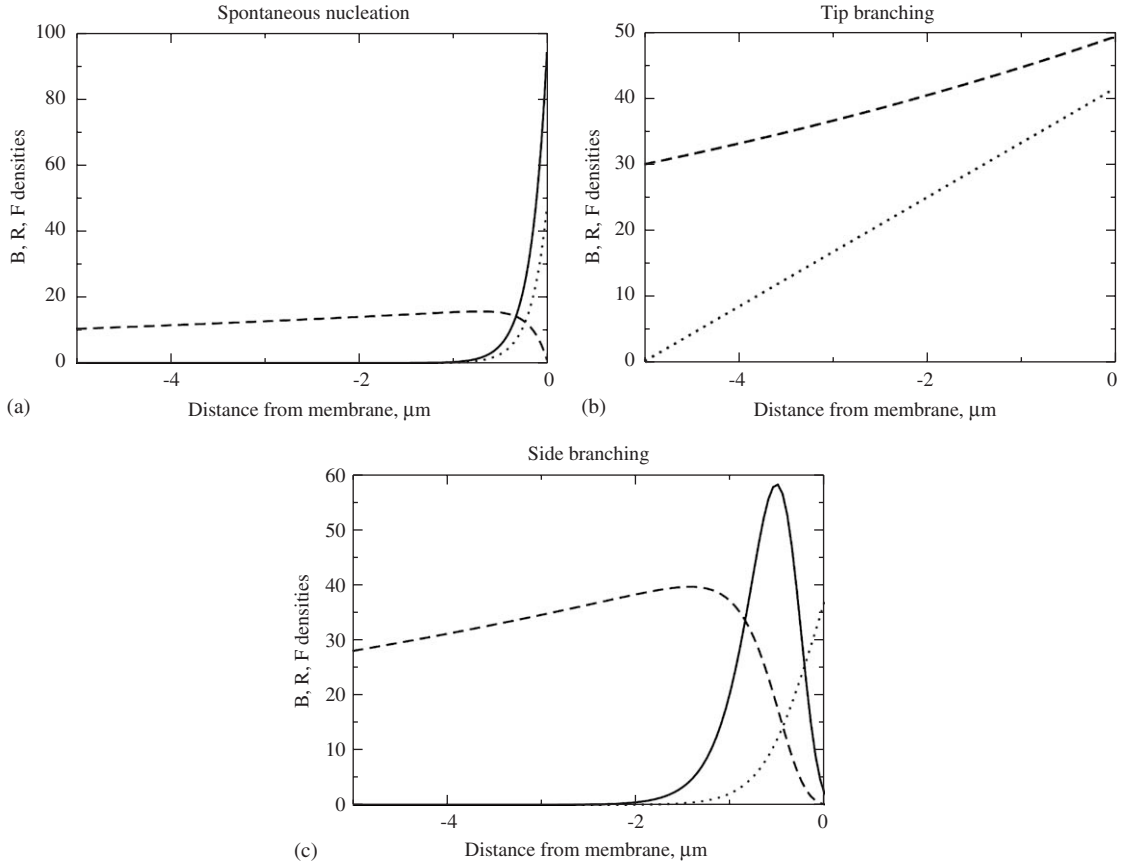

Fig. 3. Travelling wave solutions in (a) the spontaneous nucleation, (b) tip, and (c) side branching cases. Parameter values are (a) $\eta_0 = 100\,\mu m^{-1}\,s^{-1}$, (b) $\eta_1 = 1.2\,s^{-1}$, (c) $\eta_2 = 25\,\mu m^{-1}$, and all other values as in Table 1. Solid line: Barbed ends (divided by 100 in (b) to enhance visibility on the same plot), dotted line: Arp2/3 (multiplied by 50 for visibility), dashed line: filament length density. Stable nontrivial travelling wave solutions exist in all three cases. Note that Arp2/3 level is maximal at the leading edge. The profiles of barbed ends and filaments are model-dependent: in the spontaneous and tip branching cases, barbed ends are maximal at the leading edge, whereas in the side branching case, their profile peaks inside the cell, at some small distance from the membrane. In the tip branching case (b), values of η_1 that lead to a travelling wave profile produce explosive growth and an unrealistically high number of tips.

support, i.e. $B(x,0) = 0$ for $x \geqslant x_{edge}$) and found that all simulations converge after some time to a similar steady state profile. Under certain conditions, described in Section 6.4, steady state motion is established. To ensure that the boundary conditions $B(-\infty) = 0$ and $R(-\infty) = 0$ are satisfied, B and R are initially set to zero on the left boundary and are not changed during the course of the simulation. A simulation run terminates at $t = 200\,s$. Unless otherwise indicated, parameter values from Table 1 are used.

As shown in Fig. 2, the profile of barbed ends and filament length density produced by our code (dotted line) matches the analytic solution (solid line) well in the spontaneous branching case. This ensures that our simulations are accurately capturing the model dynamics and boundary conditions. Further, as shown in Fig. 7(a), the membrane speed predicted by the numerical simulations matches the analytically predicted speed (the solid line indicating the membrane speed as determined by simulations is indistinguishable from the analytically predicted membrane speed (dot–dash line)).

6. Results

6.1. Numerical results for travelling wave solutions

Figs. 2 and 3 compare the travelling wave solutions in the spontaneous, tip and side branching cases. The simulations of the spontaneous branching case agree with the analysis, while simulations of the tip and side branching extend the results to variants of the model that are not easy to treat analytically. The simulations also provide evidence for the stability of the travelling wave solutions, an issue that was not treated analytically. In all three cases, Arp2/3 has its highest value near the membrane, as expected, since Arp2/3 is activated by membrane-associated proteins. Barbed ends achieve a peak density at or close to the membrane and decay rapidly towards the rear, while filament length density peaks further away from the membrane and decays more towards the rear. In the spontaneous branching case (a), the profile of barbed ends reflects the Arp2/3 distribution since, at steady state motion, $\eta_0 r \approx \kappa b$ (from Eq. (11)). Thus the Arp2/3 profile, determined by diffusion from a source at

$x = 0$, essentially leads to the b profile. In the tip branching case (b), there is exponential growth of the barbed ends very close to the membrane where $\eta_1 R > \kappa$ and exponential decay further back. Thus, Arp2/3 is depleted at the membrane before it can diffuse into the cell. In the side branching case (c), the profile of barbed ends is a compromise between the area of high Arp2/3 and the area of high filament density. Since, by mass action, the creation of new tips is a product of the concentration of Arp2/3 and filament density, the side branching rate used in Fig. 3 ($\eta_2 = 25\,\mu\mathrm{m\,s^{-1}}$) is much higher than estimated in Section 4 due to an overestimate of the filament density near the leading edge ($\eta_2 = 1\,\mu\mathrm{m\,s^{-1}}$). In all three cases, the filament density profile is an integral of the barbed end profile, i.e. a record of barbed end motion, discounted by the actin filament decay rate.

6.2. Effect of retrograde flow and bulk flows on spatial profiles of actin and Arp2/3

To determine the effect of assumptions (i)–(iii) about the bulk flow, v_{bulk}, we ran the simulations with each of $\alpha_i = 1, 0$ for $i = 1, 2$ and compared the spatial profiles of F, B and R obtained thereby. We found that the results were nearly identical in all cases, i.e. that due to the fast Arp2/3 diffusion, assumptions about its bulk flow have little significance in terms of the results (not shown).

To determine the effect of retrograde flow on the spatial profiles, we compared simulations with nonzero v_r to results with $v_r = 0$. Again, the resulting profiles (not shown) were essentially superimposed, indicating that (at least for the parameter regime typical of keratocytes) retrograde flow has little effect on the spatial distribution of actin. The effect of retrograde flow on protrusion speed is shown in Fig. 8(d) and discussed further on.

6.3. Fitting spatial profiles to experimental data

Bailly et al. (1999) used gold-tagged gelsolin to bind to free actin filament barbed ends so that their positions could be visualized and quantified. We used their results to compare the experimental observation and the model prediction of the number of barbed ends near the leading edge. As the tip branching case produces an unrealistic explosive growth of tips, we omit this case from parameter fitting. Fig. 5 shows the best fit of the spontaneous and side branching cases to the data published in Bailly et al. (1999), when the data are recalibrated to include data points that appear to be outside the cell. The best fit was determined by using least squares, i.e., we minimized the sum of square differences between data points and predicted points. The parameter value that led to the smallest sum was chosen.

In moving coordinates, Eq. (11) for barbed ends far from the leading edge, assuming nucleation is negligible, is

$$-c\frac{\mathrm{d}b}{\mathrm{d}z} \approx -\kappa b, \quad \Rightarrow b(z) \approx \exp\left(\frac{\kappa}{c}z\right), \quad \Rightarrow \ln(b(z)) \approx \frac{\kappa}{c}z.$$

The value of κ/c can thus be estimated from a plot of the natural logarithm of the number of barbed ends as a function of distance from the leading edge, as shown in (Fig. 4). The trailing edge of the profile of barbed ends, and least squares minimization for points 0.8–1.1 μm away from the leading edge, suggests that $\kappa/c \approx 0.3$–$0.5\,\mu\mathrm{m}^{-1}$. If the leading edge were to move at close to its maximum speed, $c \approx 0.3\,\mu\mathrm{m\,s^{-1}}$, then we estimate that $\kappa \approx 0.09$–$0.15\,\mathrm{s^{-1}}$. By taking sample points closer to the leading edge, we can find higher capping rate estimates. For the profiles shown in Fig. 5, we use $\kappa = 0.1\,\mathrm{s^{-1}}$. This is surprisingly low, given that capping rates in the lamellipod are estimated to be in the range of $1\,\mathrm{s^{-1}}$. We find those values for the nucleation rate that best match the peak value of barbed ends in the experimental data to be $\eta_0 \approx 25\,\mu\mathrm{m^{-1}\,s^{-1}}$ and $\eta_2 \approx 2\,\mu\mathrm{m^{-1}\,s^{-1}}$. The ratio of η_0/η_2 is much smaller here than would be expected from our estimates in Section 4 due to an overestimate of the filament density at the leading edge. The lower absolute value of both nucleation rates is due to the lower capping rate: barbed ends are not capped as quickly so do not need to be nucleated as quickly.

Fig. 5 shows the predicted model profiles in comparison to our manually re-digitized data from Bailly et al. (1999). Both the spontaneous nucleation (Fig. 5(a)) and the side branching (Fig. 5(b)) cases are shown. Some aspects, including quantitative comparison, demonstrate differences. In Bailly et al. (1999), the membrane is destroyed during the fixation process and is not visible in the imaged sample. They assert the membrane position is determined by the presence of a dense actin meshwork, making the peak number of barbed ends occur at the membrane. However, careful scrutiny of their data reveals barbed ends lying outside the cell. They believe these barbed ends continued polymerizing after permeabilization, causing

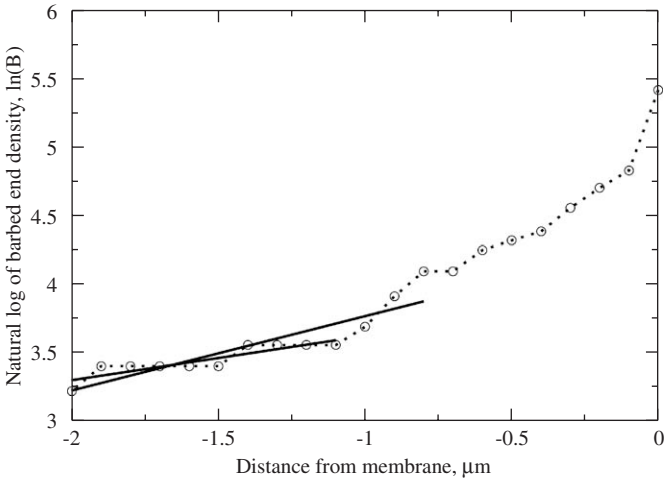

Fig. 4. Experimental data from Bailly et al. (1999) (dotted line with circles), plotted as the natural log of the number of barbed ends, ln(B), as a function of distance from the leading edge. The slope of this curve (as shown by the solid lines) is used to estimate the range of κ/c in the model, from which we estimate the effective capping rate, κ. See Section 6.3 for details.

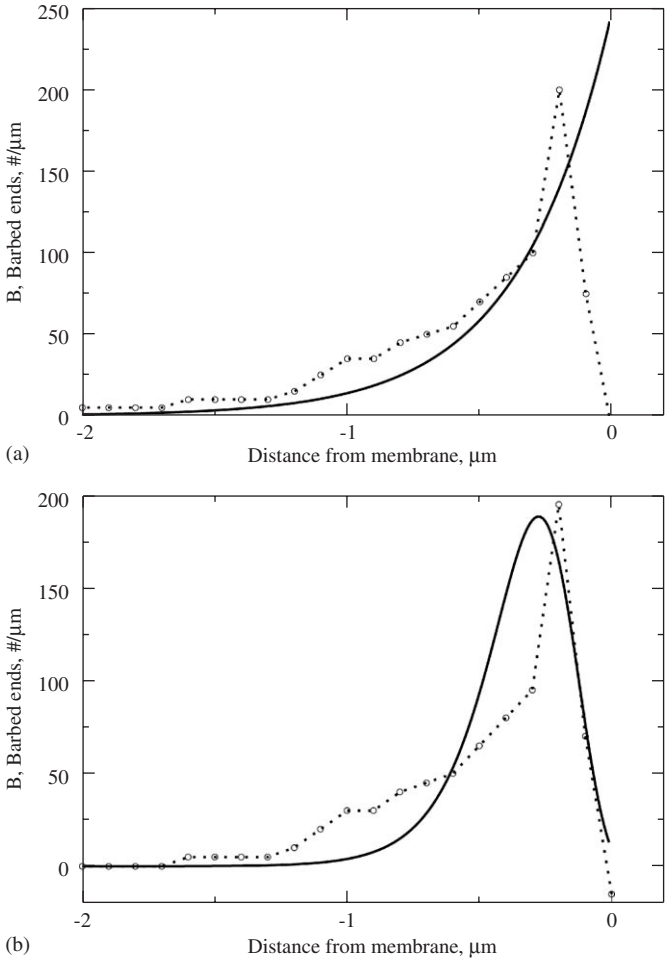

Fig. 5. Model predictions of barbed end profiles (solid line) fit to experimental data (dotted line) in the spontaneous (a) and side (b) branching cases. The experimental data are reproduced from Bailly et al. (1999), Figure 10, left panel, then shifted down and to the left. The tip branching case is omitted due to explosively high tip growth. The parameter values used to produce the profiles shown here are $\kappa = 0.1\,\mathrm{s}^{-1}$ in both plots, $\eta_0 = 25\,\mu\mathrm{m}^{-1}\mathrm{s}^{-1}$ in (a) and $\eta_2 = 2\,\mu\mathrm{m}^{-1}\mathrm{s}^{-1}$ in (b). (The parameters η_i were adjusted to fit the height of the profiles.) See Section 6.3 for a discussion of the capping rate approximation. The side branching case provides the best fit to the data.

them to grow past the membrane. Under these assumptions, the data presented in Bailly et al. (1999) are consistent with new barbed ends being generated by spontaneous branching. However, if we horizontally recalibrate their data so that non-zero data points are located inside the cell, the data are consistent with side branching. Away from the leading edge, the number of barbed ends in the experimental data decays to a non-zero value. Fluorescence imaging in live cell suggests free barbed ends are only found very close to the leading edge in motile cells (Lorenz et al., 2004; Redmond and Zigmond, 1993; Symons and Mitchison, 1991). It may be that the antibody staining used in Bailly et al. (1999) is detecting barbed ends that were previously capped by endogenous gelsolin. To account for this, we also vertically recalibrate the experimental data for the purpose of data fitting.

When the experimental data is shifted 0.2 μm to the left and down by 25 μm, the side branching case (b) matches the experimental data better, especially close to the leading edge. It is possible to shift the peak of barbed ends to better match the experimental data by increasing the capping and nucleation rates, but this causes an even sharper decay in the barbed end profile.

We compare the predicted filament density profile in the side branching case to data from Bailly et al. (1999) that has been scaled to have the same maximum value as the simulation profile. We find that a depolymerization rate of $\gamma = 0.1\,\mathrm{s}^{-1}$ provides the best fit to experimental data when the experimental data is shifted 0.4 μm to the left (Fig. 6). The profile of filament density in the side branching case is also consistent with fluorescence profiles of polymerized actin in Svitkina and Borisy (1999) and Redmond and Zigmond (1993) (not shown).

Fluorescence profiles of Arp2/3 concentration in lamellipodia have been published in Bailly et al. (1999) and Svitkina and Borisy (1999), but these include Arp2/3 that has been incorporated into branch points of the actin meshwork which does not allow for a direct comparison to this model. Overall, we find that the side branching case in this model captures the dynamics at the leading edge better than the spontaneous or tip branching cases.

6.4. Dependence of membrane speed on parameter values

We compared the dependence of membrane speed on various parameters in the three branching variants of the

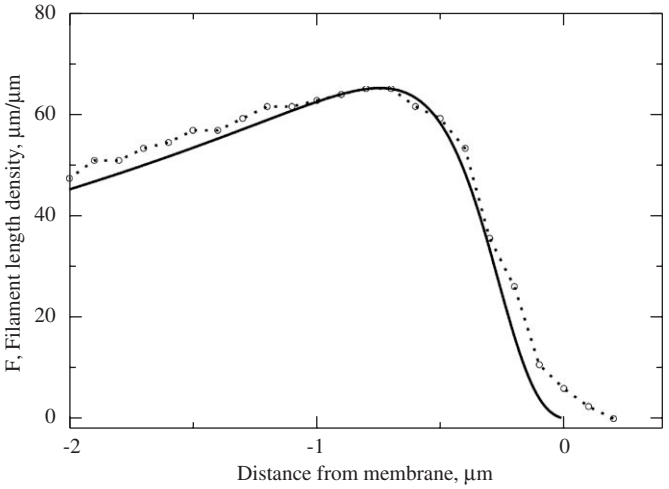

Fig. 6. Model predictions of filament density profiles (solid line) fit to experimental data (dotted line) in the side branching case. The height of the experimental data has been scaled to match the height of the simulation result. (The spontaneous and tip branching cases are not considered here, as the side branching case was found to produce the best fit to experimental data for the number of barbed ends near the leading edge; see Fig. 5). The best fit of filament density in the side branching case to the experimental data from Bailly et al. (1999) was found using $\gamma = 0.1\,\mathrm{s}^{-1}$ and shifting the experimental data 0.4 μm to the left. The simulation profile also matches favorably to fluorescence data of filament density in Svitkina and Borisy (1999).

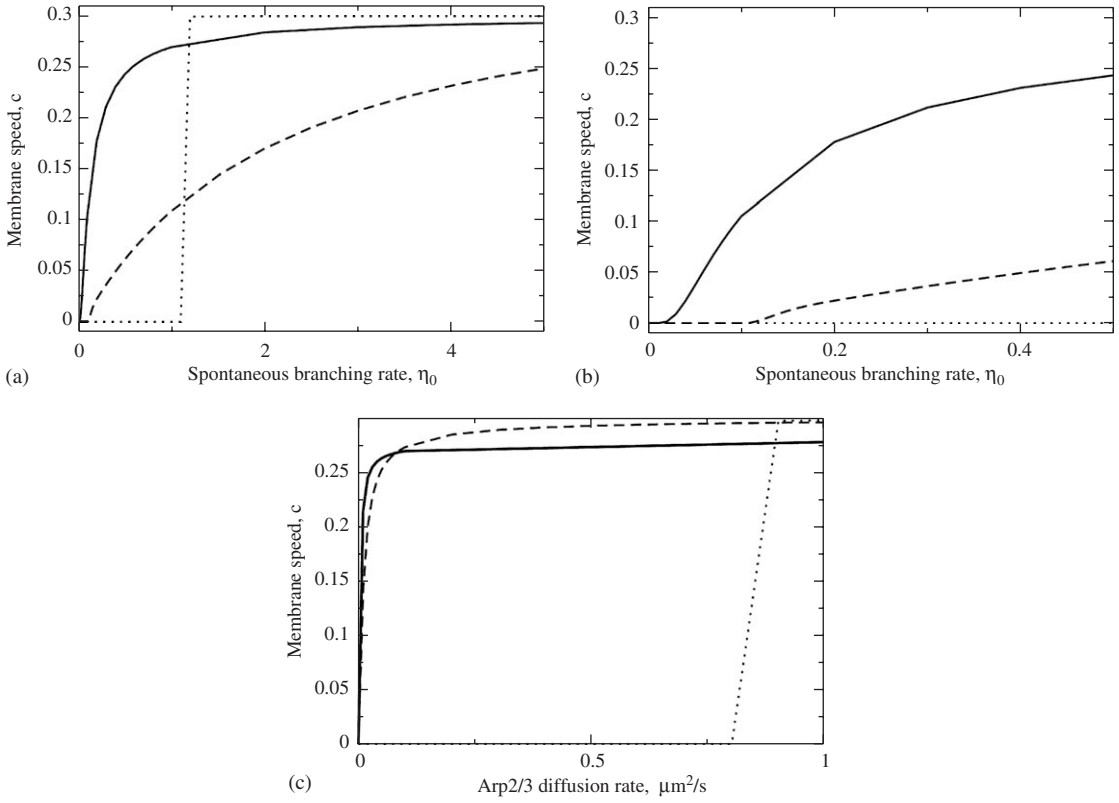

Fig. 7. Dependence of the predicted cell protrusion speed, c on parameters in the model. Speed increases as nucleation rates and Arp2/3 diffusion rate increase (with all other parameters as in Table 1). In each panel the spontaneous (solid line), tip (dotted line) and side (dashed line) branching cases are shown. (a) Speed versus nucleation rates over a range equivalent to $0 \leqslant \eta_0 \leqslant 5\,\mu m^{-1}\,s^{-1}$: Note that the rates η_1, η_2 used for tip and side branching were scaled in proportion to η_0 as discussed in Section 6.4. (The analytically predicted membrane speed in the spontaneous branching case agrees so closely with the simulation predictions that it superimposes exactly on the solid curve.) (b) Same as in (a) but for a smaller range $0 \leqslant \eta_0 \leqslant 0.5\,\mu m^{-1}\,s^{-1}$, showing that the cell stalls ($c = 0$) if nucleation rates are too low. (c) Speed c versus Arp2/3 diffusion. Membrane speed increases to a maximum value determined by Eq. (7) as Arp2/3 diffusion increases. The membrane speed increases sharply for Arp2/3 diffusion in the range $0 \leqslant D_R \leqslant 0.1\,\mu m^2\,s^{-1}$, significantly lower than our estimated Arp2/3 diffusion rate of $3\,\mu m^2\,s^{-1}$. In the spontaneous and side branching cases, the membrane speed varies smoothly as parameters of interest are varied while in the tip branching case, motion is all-or-none.

model. In general, influences that lead to a reduction in the density of barbed ends at the membrane will impede protrusion, whereas processes that lead to an increase in those barbed ends will lead to higher protrusion velocity. To base a comparison on the values of the branching rates, we chose a range of values of each of the parameters η_0, η_1, η_2 in proportion of 100:0.1:1 units explained in Section 4. In Fig. 7(a), we see that the membrane speed increases as the nucleation rate increases. This is intuitively clear since, all else being equal, for greater nucleation rates, there will be a higher density of barbed ends pushing the membrane. As shown in Fig. 7(b), in all three cases, the cell stalls if the nucleation rate is too low; very low values of nucleation cannot sustain travelling wave solutions in the model because not enough barbed ends are available to push the membrane forward. The few barbed ends pushing on the membrane are unable to overcome the membrane's resistance to movement and the cell moves at a very slow rate (from Eq. (7), the membrane speed can only be zero when $b = 0$, but for low nucleation rates, the membrane speed is very close to zero). In the spontaneous and side branching cases, the membrane speed smoothly increases as η_0, η_2 increases.

For tip branching, the membrane speed jumps from zero to near its maximum (see Eq. (7)) as η_1 varies in a small range from 1.1 to $1.2\,s^{-1}$, with all other parameter values as given in Table 1. This can be understood from Eq. (1): if $\eta_1 r < \kappa$, the solution decays to zero everywhere, whereas for $\eta_1 r > \kappa$, the solution grows exponentially. In this tip branching case, the discontinuity in the membrane speed suggests that the model is inadequate: a higher nonlinearity in the tip decay term would be required to prevent explosive growth, as, for example, with logistic growth. Based on these simulations, the tip branching case, as is, cannot be considered as a workable mechanism, and requires modification.

We find that increasing the rate of Arp2/3 diffusion causes the membrane speed to increase, up to a maximum value determined by Eq. (7). Increasing the Arp2/3 diffusion rate causes the profile of Arp2/3 to decay more slowly, allowing more barbed ends to be nucleated further into the cell, away from the leading edge. These tips then

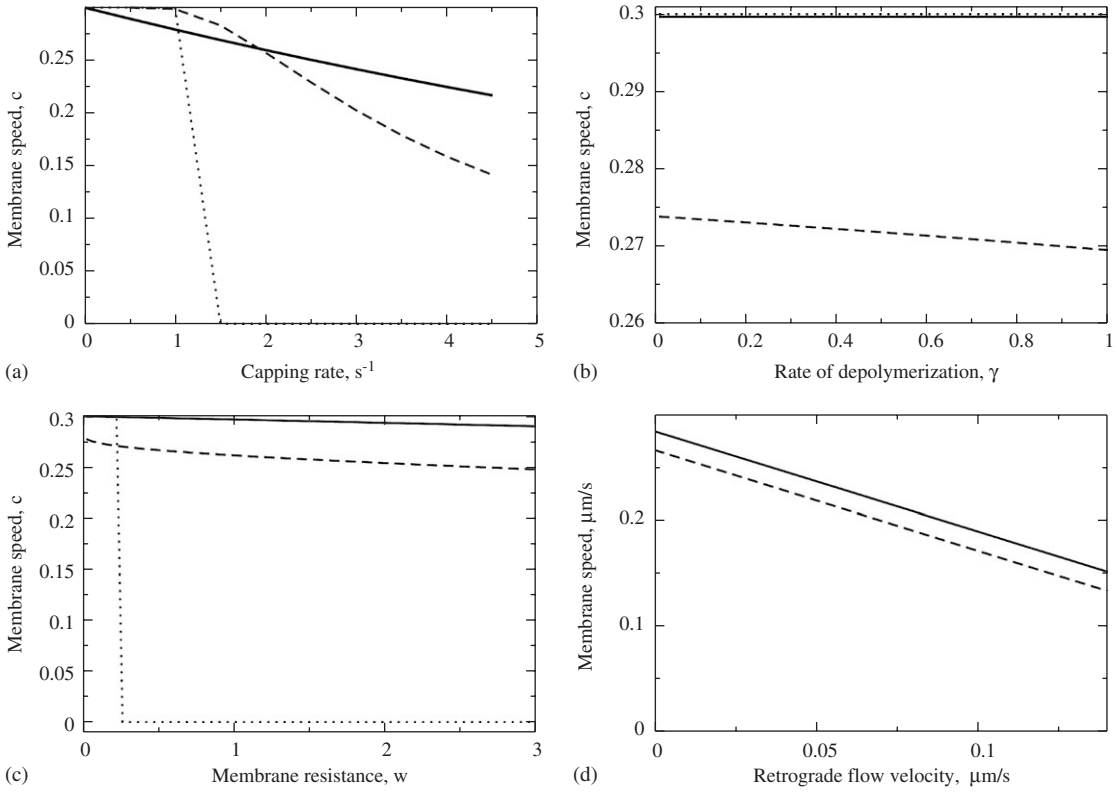

Fig. 8. Membrane speed versus (a) capping rate (s^{-1}), (b) depolymerization rate (s^{-1}), (c) membrane resistance (#/μm), and (d) retrograde flow (all other parameters as in Table 1). The spontaneous (solid line), tip (dotted line) and side (dashed line) branching cases are shown in (a–c) while the spontaneous (solid line) and side (dashed line) branching cases are shown in (d). As the depolymerization rate increases in (b), only the side branching case displays decreased membrane speed, as expected. As in Fig. 7, the membrane speed in the spontaneous and side branching cases varies smoothly as parameters of interest are varied while in the tip branching case, motion is all-or-none. As shown in (d), retrograde flow is subtractive.

grow forward to the membrane (since polymerization speed in faster than the membrane speed) where they exert force on the membrane.

Increasing membrane resistance leads to a slight decrease in membrane speed. This is consistent with the thermal ratchet equation (Eq. (7)) since membrane resistance impedes motion. Importantly, increasing the rate of filament decay causes a decrease in the membrane speed only in the side branching case as fewer filaments are available for new tip formation. The decrease in the membrane speed as the capping rate increases is due to barbed ends being capped more rapidly. As shown in Fig. 8, the speed of the cell decreases as retrograde flow increases. This is intuitively obvious, since we have modelled retrograde flow as a simple negative velocity that is superimposed on forward motion.

7. Discussion

The manner in which a cell regulates remodelling of its actin cytoskeleton to move in response to a signal has been the focus of experimental and theoretical investigations for the last decade. Experimental results demonstrate that the actin meshwork in the lamellipod has a distinct organization with most free barbed ends close to the leading edge, and nucleation of branched filaments by Arp2/3 that is activated at the leading edge. Theoretical work has investigated the length distribution of actin filaments (Carlsson, 2001; Edelstein-Keshet and Ermentrout, 2000), the relationship between the actin monomer cycle and cell speed (Mogilner and Edelstein-Keshet, 2002), and how cell shape is influenced by actin dynamics (Grimm et al., 2003). Our model builds on these efforts by studying the profile of barbed ends and filaments behind the leading edge, while taking into account spatial effects of biochemical events such as nucleation and capping. We also incorporate the "ratchet" mechanism for actin filament ends pushing forward on the membrane and generating the force that causes protrusion.

By making simplifying assumptions in constructing the model, we were able to determine an analytic formula connecting membrane speed to kinetic parameters, at least for one model variant (spontaneous nucleation). In this variant, our analytic solution for barbed end and filament length density demonstrates the existence of travelling wave solutions under a wide range of conditions. The profiles of these waves resemble observed typical density profiles in a rapidly moving cell, even though our minimal model includes only basic events such as actin filament nucleation, capping, and depolymerization. Analytic and

simulation results agree to close precision. Simulations of the side branching case, which is analytically challenging even with simplifying assumptions, also provides support for the existence of travelling wave solutions. These solutions can be interpreted as "steady state" motion of a crawling cell.

We explored distinct nucleation mechanisms (spontaneous, tip branching, or filament side-branching) to study how these would affect the observed density profiles and speeds. Tip branching in the presence of linear capping kinetics generates aberrant behavior, including explosive growth or collapse of the barbed end density close to the membrane. Thus, this variant of the model should be rejected, or modified with suitable nonlinear (e.g. logistic) growth terms to be biologically relevant. These results suggest that the tip branching of actin filaments would be a less robust or reliable mechanism than filament side branching for controlling actin density. Some papers in the literature have suggested that Arp2/3 mediates tip-branching (Pantaloni et al., 2000). Recently, experimental and theoretical evidence for side-branching has been overwhelming (see, for example, Carlsson et al., 2004, and references therein). Our simple model provides further support that the tip-branching hypothesis has some difficulties.

We investigated the dependence of the wave speed (i.e. the motility of the cell) on biochemical parameters. Under the conditions of our model, and assuming all parameters are non-zero, the model supports travelling waves in the spontaneous and side branching cases except when the nucleation rate is too small. Our results suggest that membrane speed can be smoothly varied by extracellular signals that lead to downstream adjustment of parameters such as the rate of Arp2/3 activation or the capping rate (for example, by pathways that impinge on the Rho family proteins). The case of tip branching is less relevant biologically: there we found ranges of each parameter value for which travelling wave solutions did not exist.

Finally, we used the observed actin densities to estimate some of the biochemical parameters by comparing the spatial profiles obtained from our model with experimental profiles from Bailly et al. (1999). The best fit was obtained by shifting the data 0.2 μm to the left and 25 μm down. We speculate that the horizontal shift was needed to compensate for the difficulty of identifying the true position of the membrane experimentally, as the membrane is destroyed in the process of preparing the cell for FDS imaging (Bailly et al., 1999). The vertical shift may stem from a background of barbed ends that had been capped by endogenous gelsolin prior to the experiment.

In the side branching case, the nucleation rate that provided a close fit to the experimental data ($\eta_2 = 2\,\mu m^{-1}s^{-1}$) was close to our estimate based on experimental evidence. However, the capping rate found by analysing the decay rate of the experimental data is lower than the usual capping rate of $1\,s^{-1}$ quoted in the literature (Schafer et al., 1996; Pollard et al., 2000). (But note at the leading edge the capping rate may be of order $0.1\,s^{-1}$ according to Grimm et al. (2003) and Mogilner and Edelstein-Keshet (2002).) The depolymerization rate found by comparing fluorescence data with simulation results is higher than estimates of filament depolymerization by ADF/cofilin found in the literature (Pollard et al., 2000). This discrepancy is not surprising since there are many other factors in a motile cell that sever or otherwise degrade filaments, leading to a faster decay rate than for ADF/cofilin acting alone. The depolymerization rate $\gamma = 0.1\,s^{-1}$ gives a mean filament life-time of 10 s which is consistent with experimental observations of filament turnover time in lamellipodia (Theriot and Mitchison, 1991). Shifting the experimental data for filament density from (Bailly et al., 1999) 0.4 μm to the left provided the best fit. While the data are taken from a different cell, the cell is prepared in the same manner as described for the barbed end data, requiring destruction of the cell membrane. We cannot dismiss the fact that our simple model may fail to capture some essential processes that would account for the discrepancy between model and experimental data. This suggests that further investigation of capping dynamics near the leading edge, perhaps by modifying this model to include a distinct capping zone, is in order.

Our model also attempts to address the effect of retrograde flow on the characteristic actin densities seen in motile cells. In other slow moving cell types, such as neural growth cones, retrograde flow is rapid ($\sim$2–10 $\mu m\,min^{-1}$, Jurado et al., 2005; Lin et al., 1996) compared to observed rates in keratocytes ($\sim$1–3 $\mu m\,min^{-1}$ Ponti et al., 2004; Jurado et al., 2005; Vallotton et al., 2005). In the center forward part of a keratocyte lamellipod, retrograde flow is so small ($0.01\,\mu m\,s^{-1}$, Jurado et al., 2005; Vallotton et al., 2005) that it has a negligible effect on actin spatial profiles and membrane speed predicted by the model, i.e. it does not appear to significantly affect our results.

Many known effects that play an important role in the motility of actual cells have not been included in our model. The adhesion and contractility of cells (such as fibroblasts) was not considered. This makes the model more suitable for describing the gliding motility of the fish keratocytes. The cycle of actin monomers and the depletion of those monomers at the leading edge was also left out (but see the treatment in Mogilner and Edelstein-Keshet, 2002). The spatial variation in kinetic parameters (e.g. reduced capping near the membrane, variations in the rate of filament depolymerization over the lamellipodium as filaments age, etc.) were also not considered. For instance, the spatial profiles of capping protein or ADF/cofilin (Svitkina and Borisy, 1999) could be incorporated into our model to give a more biologically realistic spatial dependence to capping and filament decay rates. In an extension of this work, the interplay with other regulatory agents (e.g. Rho-family GTP-ases), the effect of filament orientations, and extension to a moving cell in 2D will be explored.

Acknowledgments

During the preparation of this paper, L.E.-K. and E.N.C. were supported by the Natural Sciences and Engineering Research Council (NSERC, Canada), A.T.D. was supported partly by the National Science Foundation (NSF, USA; subcontract to LEK of grant DMS-0240770 to Anders Carlsson (WU)) and partly by the Mathematics of Information Technology and Complex Systems (MITACS, Canada). G.B.E. was supported by NSF.

References

Abraham, V.C., Krishnamurthi, V., Taylor, D.L., Lanni, F., 1999. The actin-based nanomachine at the leading edge of migrating cells. Biophys. J. 3 (77), 1721–1732.

Amann, K.J., Pollard, T.D., 2001. Direct real-time observation of actin filament branching mediated by Arp2/3 complex using total internal reflection fluorescence microscopy. Proc. Natl Acad. Sci. USA 26 (98), 15009–15013.

Bailly, M., Macaluso, F., Cammer, M., Chan, A., Segall, J.E., Condeelis, J.S., 1999. Relationship between Arp2/3 complex and the barbed ends of actin filaments at the leading edge of carcinoma cells after epidermal growth factor stimulation. J. Cell Biol. 145 (2), 331–345.

Bailly, M., Ichetovkin, I., Grant, W., Zebda, N., Machesky, L.M., Segall, J.E., Condeelis, J., 2001. The F-actin side binding activity of the Arp2/3 complex is essential for actin nucleation and lamellipod extension. Curr. Biol. 8 (11), 620–625.

Carlsson, A.E., 2001. Growth of branched actin networks against obstacles. Biophys. J. 4 (81), 1907–1923.

Carlsson, A.E., Wear, M.A., Cooper, J.A., 2004. End versus side branching by Arp2/3 complex. Biophys. J. 2 (86), 1074–1081.

DiNubile, M.J., Huang, S., 1997. High concentrations of phosphatidylinositol-4,5-bisphosphate may promote actin filament growth by three potential mechanisms: inhibiting capping by neutrophil lysates, severing actin filaments and removing capping protein-beta(2) from barbed ends. Biochim. Biophys. Acta—Mol. Cell Res. 3 (1358), 261–278.

Edelstein-Keshet, L., Ermentrout, G.B., 2000. Models for spatial polymerization dynamics of rod-like polymers. J. Math. Biol. 1 (40), 64–96.

Falet, H., Hoffmeister, K.M., Neujahr, R., Italiano, J.E., Stossel, T.P., Southwick, F.S., Hartwig, J.H., 2002. Importance of free actin filament barbed ends for Arp2/3 complex function in platelets and fibroblasts. Proc. Natl Acad. Sci. USA 26 (99), 16782–16787.

Feinberg, J., Kwiatek, O., Astier, C., Diennet, S., Mery, J., Heitz, F., Benyamin, Y., Roustan, C., 1998. Capping and dynamic relation between domains 1 and 2 of gelsolin. J. Pept. Sci. 2 (4), 116–127.

Fujiwara, I., Suetsugu, S., Uemura, S., Takenawa, T., Ishiwata, S., 2002. Visualization and force measurement of branching by Arp2/3 complex and N-WASP in actin filament. Biochem. Biophys. Res. Commun. 5 (293), 1550–1555.

Grimm, H.P., Verkhovsky, A.B., Mogilner, A., Meister, J.J., 2003. Analysis of actin dynamics at the leading edge of crawling cells: implications for the shape of keratocyte lamellipodia. Eur. Biophys. J. Biophys. Lett. 6 (32), 563–577.

Henson, J.H., Svitkina, T.M., Burns, A.R., Hughes, H.E., MacPartland, K.J., Nazarian, R., Borisy, G.G., 1999. Two components of actin-based retrograde flow in sea urchin coelomocytes. Mol. Biol. Cell 12 (10), 4075–4090.

Huang, M., Yang, C., Schafer, D.A., Cooper, J.A., Higgs, H.N., Zigmond, S.H., 1999. Cdc42-induced actin filaments are protected from capping protein. Curr. Biol. 17 (9), 979–982.

Jurado, C., Haserick, J.R., Lee, J., 2005. Slipping or gripping? Fluorescent speckle microscopy in fish keratocytes reveals two different mechanisms for generating a retrograde flow of actin. Mol. Biol. Cell 2 (16), 507–518.

Kurner, J., Medalia, O., Linaroudis, A.A., Baumeister, W., 2004. New insights into the structural organization of eukaryotic and prokaryotic cytoskeletons using cryo-electron tomography. Exp. Cell Res. 1 (301), 38–42.

Lambrechts, A., Van Troys, M., Ampe, C., 2004. The actin cytoskeleton in normal and pathological cell motility. Int. J. Biochem. Cell Biol. 10 (36), 1890–1909.

Lin, C.H., Espreafico, E.M., Mooseker, M.S., Forscher, P., 1996. Myosin drives retrograde F-actin flow in neuronal growth cones. Neuron 4 (16), 769–782.

Lorenz, M., DesMarais, V., Macaluso, F., Singer, R.H., Condeelis, J., 2004. Measurement of barbed ends, actin polymerization, and motility in live carcinoma cells after growth factor stimulation. Cell Motil. Cytoskeleton 4 (57), 207–217.

Mandato, C.A., Bement, W.M., 2003. Actomyosin transports microtubules and microtubules control actomyosin recruitment during Xenopus oocyte wound healing. Curr. Biol. 13 (12), 1096–1105.

Mogilner, A., Edelstein-Keshet, L., 2002. Regulation of actin dynamics in rapidly moving cells: a quantitative analysis. Biophys. J. 3 (83), 1237–1258.

Mogilner, A., Oster, G., 1996. Cell motility driven by actin polymerization. Biophys. J. 6 (71), 3030–3045.

Mogilner, A., Oster, G., 2003. Polymer motors: pushing out the front and pulling up the back. Curr. Biol. 18 (13), R721–R733.

Pantaloni, D., Boujemaa, R., Didry, D., Gounon, P., Carlier, M.F., 2000. The Arp2/3 complex branches filament barbed ends: functional antagonism with capping proteins. Nat. Cell Biol. 7 (2), 385–391.

Pollard, T.D., Borisy, G.G., 2003. Cellular motility driven by assembly and disassembly of actin filaments. Cell 4 (112), 453–465.

Pollard, T.D., Blanchoin, L., Mullins, R.D., 2000. Molecular mechanisms controlling actin filament dynamics in nonmuscle cells. Annu. Rev. Biophys. Biomolecular Struct. 29, 545–576.

Ponti, A., Machacek, M., Gupton, S.L., Waterman-Storer, C.M., Danuser, G., 2004. Two distinct actin networks drive the protrusion of migrating cells. Science 5691 (305), 1782–1786.

Ponti, A., Matov, A., Adams, M., Gupton, S., Waterman-Storer, C.M., Danuser, G., 2005. Periodic patterns of actin turnover in Lamellipodia and lamellae of migrating epithelial cells analyzed by quantitative Fluorescent Speckle Microscopy. Biophys. J. 5 (89), 3456–3469.

Redmond, T., Zigmond, S.H., 1993. Distribution of F-actin elongation sites in lysed polymorphonuclear leukocytes parallels the distribution of endogenous F-actin. Cell Motil. Cytoskeleton 1 (26), 7–18.

Schafer, D.A., Jennings, P.B., Cooper, J.A., 1996. Dynamics of capping protein and actin assembly in vitro: uncapping barbed ends by polyphosphoinositides. J. Cell Biol. 1 (135), 169–179.

Small, J.V., Herzog, M., Anderson, K., 1995. Actin filament organization in the fish keratocyte lamellipodium. J. Cell Biol. 5 (129), 1275–1286.

Small, J.V., Stradal, T., Vignal, E., Rottner, K., 2002. The lamellipodium: where motility begins. Trends Cell Biol. 3 (12), 112–120.

Suetsugu, S., Miki, H., Takenawa, T., 2002. Spatial and temporal regulation of actin polymerization for cytoskeleton formation through Arp2/3 complex and WASP/WAVE proteins. Cell Motil. Cytoskeleton 51 (3), 113–122.

Svitkina, T.M., Borisy, G.G., 1999. Arp2/3 complex and actin depolymerizing factor cofilin in dendritic organization and treadmilling of actin filament array in lamellipodia. J. Cell Biol. 5 (145), 1009–1026.

Svitkina, T.M., Verkhovsky, A.B., McQuade, K.M., Borisy, G.G., 1997. Analysis of the actin-myosin II system in fish epidermal keratocytes: mechanism of cell body translocation. J. Cell Biol. 139 (2), 397–415.

Symons, M.H., Mitchison, T.J., 1991. Control of actin polymerization in live and permeabilized fibroblasts. J. Cell Biol. 3 (114), 503–513.

Theriot, J.A., Mitchison, T.J., 1991. Actin microfilament dynamics in locomoting cells. Nature 6331 (352), 126–131.

Tojima, T., Ito, E., 2004. Signal transduction cascades underlying de novo protein synthesis required for neuronal morphogenesis in differentiating neurons. Prog. Neurobiol. 3 (72), 183–193.

Vallotton, P., Gupton, S.L., Waterman-Storer, C.M., Danuser, G., 2004. Simultaneous mapping of filamentous actin flow and turnover in migrating cells by quantitative fluorescent speckle microscopy. Proc. Natl Acad. Sci. USA 26 (101), 9660–9665.

Vallotton, P., Danuser, G., Bohnet, S., Meister, J.J., Verkhovsky, A.B., 2005. Tracking retrograde flow in keratocytes: news from the front. Mol. Biol. Cell 3 (16), 1223–1231.

Verkhovsky, A.B., Chaga, O.Y., Schaub, S., Svitkina, T.M., Meister, J.J., Borisy, G.G., 2003. Orientational order of the lamellipodial actin network as demonstrated in living motile cells. Mol. Biol. Cell 11 (14), 4667–4675.

Wiesner, S., Helfer, E., Didry, D., Ducouret, G., Lafuma, F., Carlier, M.F., Pantaloni, D., 2003. A biomimetic motility assay provides insight into the mechanism of actin-based motility. J. Cell Biol. 3 (160), 387–398.

Wood, W., Martin, P., 2002. Structures in focus—filopodia. Int. J. Biochem. Cell Biol. 7 (34), 726–730.